Catalytic Mechanism and Substrate Specificity of the β-Subunit of the Voltage-Gated Potassium Channel†

Srinivas M. Tipparaju, Oleg A. Barski, Sanjay Srivastava, and Aruni Bhatnagar*

Division of Cardiology, Department of Medicine, Institute of Molecular Cardiology, University of Louisville, Louisville, Kentucky 40202

Received February 21, 2008; Revised Manuscript Received June 10, 2008

ABSTRACT: The β-subunits of voltage-gated potassium (Kv) channels are members of the aldo-keto reductase (AKR) superfamily. These proteins regulate inactivation and membrane localization of Kv1 and Kv4 channels. The Kvβ proteins bind to pyridine nucleotides with high affinity; however, their catalytic properties remain unclear. Here we report that recombinant rat Kvβ2 catalyzes the reduction of a wide range of aldehydes and ketones. The rate of catalysis was slower (0.06−0.2 min^{-1}) than those of most other AKRs but displayed the expected hyperbolic dependence on substrate concentration, with no evidence of allosteric cooperativity. Catalysis was prevented by site-directed substitution of Tyr-90 with phenylalanine, indicating that the acid−base catalytic residue, identified in other AKRs, has a conserved function in Kvβ2. The protein catalyzed the reduction of a broad range of carbonyls, including aromatic carbonyls, electrophilic aldehydes and prostaglandins, phospholipids, and sugar aldehydes. Little or no activity was detected with carbonyl steroids. Initial velocity profiles were consistent with an ordered bi-bi rapid equilibrium mechanism in which NADPH binding precedes carbonyl binding. Significant primary kinetic isotope effects (2.0−3.1) were observed under single- and multiple-turnover conditions, indicating that the bond-breaking chemical step is rate-limiting. Structure−activity relationships with a series of para-substituted benzaldehydes indicated that the electronic interactions predominate during substrate binding and that no significant charge develops during the transition state. These data strengthen the view that Kvβ proteins are catalytically active AKRs that impart redox sensitivity to Kv channels.

Most eukaryotic cells express a diverse range of voltage-gated potassium (Kv)[1] channels (*1*). In excitable cells, such as nerves and muscles, Kv channels regulate the generation and duration of action potential, firing patterns, pacemaking, and neurotransmitter release (*2–4*). In nonexcitable cells, these channels participate in volume regulation, hormonal secretion, proliferation, and apoptosis (*5–8*). Native mammalian Kv channels are large macromolecular complexes composed of four pore-forming transmembrane proteins (Kv α-subunits) that regulate K^+ efflux. The cytosolic domains of the Kv1 and -4 α-subunits associate with auxiliary β-subunits that regulate channel assembly and function. In mammals, three distinct Kvβ genes have been identified. These genes encode proteins with a highly conserved C-terminus and a variable N-terminal domain. The conserved C-terminus of Kvβ proteins folds into an $(\alpha/\beta)_8$ or triose-phosphate isomerase (TIM) barrel motif, which is the most common structural scaffolding among enzymes involved in metabolism and biosynthesis (*9*). The TIM barrel also forms an efficient fold for high-affinity binding of flavin and pyridine nucleotides that participate in catalyzing oxidation−reduction reactions (*9*). The TIM barrel structure of Kvβ proteins bears a strong structural resemblance and sequence similarity to proteins of the aldo-keto reductase (AKR) superfamily, and the catalytic features of the AKR active site are conserved in the C-terminal domain of Kvβ proteins (*10–12*). On the basis of this homology, the Kvβ proteins have been classified as a distinct family (AKR6) within the AKR superfamily of proteins (*13*).

Our previous studies show that like other AKRs, the Kvβ proteins bind to pyridine nucleotides with high affinity (*14, 15*). We have found that binding of reduced nucleotides supports N-terminally mediated inactivation of Kvα currents by Kvβ, whereas oxidized nucleotides remove inactivation of K^+ currents generated by Kv αβ-subunits (*16*). These observations support the notion that the β-subunits impart metabolic sensitivity to Kv currents. Such coupling might allow the Kv channel to sense changes in cell metabolism and oxygenation (*17*). Nevertheless, it remains unclear whether binding of pyridine nucleotide to Kvβ proteins by itself is required for the regulation of Kv activity or if catalysis is necessary to change the redox state of the nucleotide bound to Kvβ. Clearly, further studies on the catalytic activity and substrate specificity of Kvβ are required to understand how it regulates Kv function.

† This work was partly supported by NIH Grants HL-544771, HL-59378, and ES-11860 (to A.B.) and HL-089372 (to O.A.B.) and a fellowship from the American Heart Association (0425439B, to S.M.T.).

* To whom correspondence should be addressed: Division of Cardiology, Department of Medicine, University of Louisville, Louisville, KY 40202. Telephone: (502) 852-5966. Fax: (502) 852-3663. E-mail: aruni@louisville.edu.

[1] Abbreviations: 4-NB, 4-nitrobenzaldehyde; 4-NAP, 4-nitroacetophenone; 4-HNE, 4-hydroxy-*trans*-2-nonenal; DHN, 1,4-dihydroxy-*trans*-2-nonene; 4-ONE, 4-oxo-*trans*-2-nonenal; Kv, voltage-gated potassium; Kvβ, voltage-gated potassium channel β-subunit; AKR, aldo-keto reductase; SEM, standard error of the mean.

10.1021/bi800301b CCC: $40.75
Published on Web 08/02/2008

Several lines of evidence suggest that Kvβ proteins are catalytically active and exhibit AKR properties. The AKR active site is conserved in Kvβ proteins, and the catalytic residues are positioned for efficient carbonyl binding. Moreover, mutations at the active site markedly affect the inactivating properties of Kvβ (*15, 18, 19*). Indeed, weak catalytic activity of Kvβ2 with aromatic aldehydes has been reported previously (*18*). Nevertheless, the catalytic and kinetic mechanisms of the protein remain poorly understood, and its substrate specificity is unknown. Specifically, it is not clear whether the protein displays cooperativity, which steps limit the overall catalytic rate, and which structural features facilitate substrate binding to the active site. This study was therefore designed to identify the reaction sequence, to determine the kinetic mechanism of catalysis, and to examine the substrate specificity of the protein. Our results show that Kvβ follows a rapid equilibrium bi-bi ordered reaction mechanism. These properties may be important aspects of Kvβ function.

EXPERIMENTAL PROCEDURES

Mutagenesis and Expression of Kvβ2. The cDNA encoding rat Kvβ2 (rKvβ2) was provided by M. Li (Johns Hopkins University, Baltimore, MD). The construct for bacterial expression of rKvβ2 (NP_059000) with a His tag at its N-terminus in the pET28a vector was generated as described previously (*14*). Site-directed mutagenesis was performed directly in a pET28a vector using a QuikChange XL site-directed mutagenesis kit (Stratagene). The sequences of the PCR primers were 5′-CGATACGGCGGAGGTCTTCG-CAGCTGGCAAGGCTG-3′ (forward) and 5′-CAGCCT-TGCCAGCTGCGAAGACCTCCGCCGTATCG-3′ (reverse). The complete sequence of the mutated Kvβ2 insert was confirmed by DNA sequencing. Wild-type and mutant Kvβ2 were expressed in the BL-21(DE3) strain of *Escherichia coli* and purified to homogeneity as described previously (*14*).

Protein Purification. The C-terminal domain of Kvβ2 (amino acids 39−367) was expressed with a His tag at its N-terminus in the BL-21 strain of *E. coli*. The bacterial pellet was lysed in ice-cold binding buffer containing 150 mM NaCl, 20 mM Tris, and 5 mM imidazole (pH 7.9). The supernatant was incubated with Ni-affinity agarose beads (Qiagen) for 2−3 h at 4 °C. The Ni column was washed with binding buffer with 10 times the bed volume, and the protein was eluted with imidazole. A small volume from each eluted fraction (2 μL) was separated by SDS−PAGE. The purified proteins were stored at 4 °C in 0.2 M potassium phosphate buffer (pH 7.4) and used within 4−6 weeks. The concentration of the protein was measured using Bradford's assay (*20*).

NADPH Binding Studies. Binding of NADPH to WT or Y90F Kvβ2 was assessed by fluorescence titration as described previously (*14*). Briefly, the protein (15 μg) was equilibrated in 2 mL of 0.2 M potassium phosphate buffer at room temperature for 10 min, and changes in fluorescence were measured using an excitation wavelength of 280 nm and emission at 340 nm. Aliquots of NADPH were added, and changes in emission were recorded. Fluorescence changes obtained by titrating tryptophan with NADPH were used to correct for the inner filter effect (*14*). Dissociation constants were calculated using the following equation:

$$\Delta F = \Delta F_{max}\mathrm{NADPH}/(K_d + \mathrm{NADPH}) \quad (1)$$

Activity Measurements in Multiple- and Single-Turnover Mode. Activity assays were performed in multiple- or single-turnover mode (*18, 21*). Multiple turnovers were assessed in quartz microcuvettes containing, in a volume of 250 μL, Kvβ2 (15−20 μM), NADPH (150 μM), and 0.2 M phosphate (pH 7.4) incubated at 37 °C. The reaction was started by adding the substrate. Loss of NADPH was monitored by following changes in absorbance at 340 nm for 15 min on a spectrophotometer (Cary Varian 50). For the measurement of single-turnover activity, the Kvβ2 protein was pre-equilibrated at 37 °C and the reaction was initiated by adding the substrate (0.2−2 mM). The reaction was monitored continuously by measuring changes in A_{360} for 30−60 min at 37 °C to follow the oxidation of NADPH bound to Kvβ2.

Synthesis of Deuterated NADPH. NADPH and NADPD were synthesized by using alcohol dehydrogenase from *Thermoanaerobium brockii* (Sigma Chemical Co.) as described previously (*22*). For synthesis, alcohol dehydrogenase 2U (1.21 mg) was incubated with 2 mM $NADP^+$ in 50 mM Tris-HCl (pH 7.8) and 300 mM 2-propanol or 2-propanol-d_8 (Sigma Chemical Co.) for 1 h at 40 °C. The progress of the reaction was monitored by measuring changes in absorbance at 340 nm. After completion, the reaction mixture was loaded on an anion-exchange column pre-equilibrated with 20 mM Tris-HCl (pH 9.0). The column was washed with 25−30 mL of 20 mM Tris-HCl (pH 9.0), and the reduced cofactor NADPH/D was eluted by using 250 mM NaCl and 50 mM Tris (pH 7.8). The absorbance of the eluted fractions at 260 and 340 nm was recorded. Fractions with an A_{260}/A_{340} ratio of >2.4 were pooled, and the pH of the mixture was adjusted to 9.0 with NaOH. Synthesized pyridine nucleotides were stored at −80 °C until further use.

Nucleotide Replacement Experiments. The Kvβ2 protein, purified from bacteria, remains tightly bound to NADPH, and the cofactor is not removed by dialysis. Hence, for kinetic isotope effect studies, NADPH bound to Kvβ was removed by oxidizing it to $NADP^+$, which dissociates from the protein more readily than NADPH. For this, Kvβ2, purified from bacteria, was incubated with 4-nitrobenzaldehyde (600 μM), and the disappearance of NADPH was monitored at 360 nm. After the reaction had been driven to completion, the reaction mixture was transferred to a dialysis cassette (10000 Da cutoff, Pierce) and dialyzed against 0.2 M potassium phosphate (pH 7.4) at 4 °C for 16−20 h. The protein was then incubated with reagent NADPH or NADPD for 30 min at 4 °C. Excess coenzyme was removed by equilibrium dialysis. The progress of the reaction was monitored at each step by measuring changes in absorbance at 360 nm.

Kinetic Isotope Effects. To study kinetic isotope effects, 150 μM synthesized NADPH or NADPD was mixed with 20 μM Kvβ2 in 0.2 M potassium phosphate (pH 7.4) at 37 °C. The enzyme reaction was started by adding varying concentrations (0.1−2 mM) of the substrate. Coenzyme oxidation was monitored at 340 nm for 15 min at 37 °C. For the calculation of velocity, only the initial, linear part of the reaction was used. Kinetic isotope effects on single-turnover reactions were calculated from the rate of oxidation of NADPH or NADPD bound to Kvβ2 measured at 37 °C for 30 min after the addition of the substrate.

Product Identification. Reduction of phospholipid aldehyde 1-palmitoyl-2-(5-oxovaleroyl)-*sn*-glycero-3-phosphatidylcholine (POVPC) to 1-palmitoyl-2(5)-hydroxyvaleroyl-*sn*-glycero-3-phosphorylcholine (PHVPC) by Kvβ2 was followed by electrospray mass spectrometry (ESI^+/MS) as described previously (*23*). The reaction mixture containing 35 μM Kvβ2, 150 μM NADPH, and 80 μM POVPC was incubated at 37 °C for 3 h. Additional NADPH was added to the reaction mixture at 45 min intervals. The reaction was stopped after 3 h, and the phospholipid in the mixture was extracted by using the Bligh and Dryer (*24*) procedure. For ESI^+/MS analysis, a MicroMass ZMD 2000 mass spectrophotometer (Waters-Micromass, Milford, MA) was used. The injection solvent was a 2:1 (v/v) methanol/chloroform mixture containing 1.0% acetic acid in positive ionization mode and a 2:1 (v/v) methanol/chloroform mixture containing 10 mM ammonium hydroxide in negative ionization mode. Samples were injected into the spectrometer using a Harvard syringe pump at a flow rate of 25 μL/min. The ESI^+/MS operating parameters were as follows: capillary voltage, 3.38 kV; cone voltage, 25 V; extractor voltage, 9 V; RF lens voltage, 0.9 V; and source block and desolvation temperatures, 100 and 200 °C, respectively. Nitrogen was used as the nebulizer gas at a flow rate of 3.4 L/h. Spectra were acquired at a rate of 275 atomic mass units per second over the mass range of 2−1000 atomic mass units and were averaged over a period of 5 min or 100 scans (*23*).

HPLC Analysis. Reagent 4-hydroxy-*trans*-2-nonenal (4-HNE) and 1,4-dihydroxynonenal (DHN) were synthesized as described previously (*25*). The 4-oxo-2-nonenol was synthesized by reducing 4-oxo-2-nonenal (4-ONE) with aldose reductase (*25*). Reagent 4-HNE, 4-ONE, DHN, and 4-oxo-2-nonenol were separated by HPLC using a Varian reverse phase ODS C_{18} column pre-equilibrated with 0.1% aqueous trifluoroacetic acid. The compounds were eluted using a gradient consisting of solvent A (0.1% aqueous trifluoroacetic acid) and solvent B (100% acetonitrile) at a flow rate of 1 mL/min. The gradient was established such that the level of solvent B reached 26% in 30 min and was held at this value for 10 min. Over the next 10 min, the level of solvent B reached 60%. After an additional 5 min, it reached 100% and was held at this value for 10 min. Under these conditions, DHN, 4-oxo-2-nonenol, 4-HNE, and 4-ONE eluted with retention times of 31, 37, 43, and 53 min, respectively.

Analysis of the Reduced Product by Gas Chromatography−Mass Spectrometry (GC−MS). HPLC-purified peak II was extracted in dichloromethane and dried under nitrogen. The samples were derivatized with 50 μL of BSTFA−TMS [*N*,*O*-bis(trimethylsilyl)trifluoroacetamide with trimethylchlorosilane] for 5 min at 80 °C. An aliquot (1 μL) of the mixture was utilized for gas chromatography−electron impact ionization mass spectrometry (GC−EI-MS) analysis. GC−EI-MS analysis was performed using an HP-6890/HP5973 GS/MS system (Hewlett-Packard, Palo Alto, CA). Compounds were separated on a bonded phase capillary column (DB-5MS, 30 m × 0.25 mm × 0.25 μm film thickness from J&W Scientific, Folson, CA). The GC injection port and interface temperature were set at 280 °C. Injections were made in the splitless mode with the inlet port purged for 1 min following injection. The GC oven temperature was held initially at 100 °C for 1 min, then increased at a rate of 10 °C/min to 280 °C, and then held there for 5 min. Under these conditions, the retention time of 4-oxo-2-nonenol was 8.06 min.

Hammett Plot Analysis. The kinetic constants, K_m and k_{cat}, were obtained with the series of benzaldehyde compounds. For each para-substituted benzaldehyde, values for electronic (σ^+), steric (υ), and hydrophobic (Π) parameters were obtained from published literature (*26–28*). The log k_{cat}, log K_m, or log k_{cat}/K_m values were plotted versus σ^+, and the correlation coefficients were obtained from multivariate weighted analysis as described previously (*22, 29*) for the following equation using SAS 9.1:

$$\log k_{cat}/K_m, \log k_{cat}, \text{ or } \log K_m = \rho\sigma^+ + A\upsilon + B\Pi + C \quad (2)$$

where σ^+ is the Hammett constant for electronic effects, Π is the Hansch constant for the hydrophobic interactions, and υ is the steric constant. ρ, A, B, and C are parameter coefficients.

Data Analysis. Steady-state kinetic constants k_{cat} and K_m were calculated by fitting the Michaelis−Menten equation directly in the hyperbolic form to the initial velocities using the Marquardt−Levenberg algorithm. For nonlinear regression analysis, SigmaPlot 9.0 was used. Single-turnover traces were analyzed using a single-exponential decay equation:

$$A_{360} = ae^{-k_{trans}t} + b \quad (3)$$

Calculated pseudo-first-order rate constants, k_{trans}, were then plotted against substrate concentration and analyzed using nonlinear regression analysis. Kinetic isotope effects were calculated from the initial velocities obtained with NADPH and NADPD at various substrate concentrations using the following equations:

$$\upsilon = V_M A/[K_m(1 + F_i E_{k_{cat}/K_m}) + A(1 + F_i E_{k_{cat}})] \quad (4)$$

$$\upsilon = V_M A/[(K_m + A)(1 + F_i E)] \quad (5)$$

where A is the concentration of aldehyde substrate, F_i is the fraction of deuterium in the NADPH/NADPD cofactor, and $E_{k_{cat}}/K_m$ and $E_{k_{cat}}$ are the isotope effects minus 1 on k_{cat}/K_m and k_{cat}, respectively. Equation 5 assumes that $E_{k_{cat}}/K_m = E_{k_{cat}}$. Multivariate regression analysis was performed using SigmaPlot 9.0. Data are presented as means ± SEM. Intergroup comparisons were made using the unpaired Student's *t*-test, and a P of <0.05 was considered to be statistically significant.

RESULTS

Kvβ2-Mediated Catalysis. To determine whether the purified Kvβ2 protein was enzymatically active, fundamental properties of its catalysis were determined. For this, the pH and ionic dependence of the reaction and the dependence of the reaction velocity on the concentration of the protein and its substrates were studied. In addition, we also established the identity of the acid−base catalyst and authenticated the formation of reduced products generated by the protein. In the first series of experiments, the rate of NADPH reduction was measured using 4-nitrobenzaldehdye (4-NB) as a model AKR substrate. When the sample was incubated with 1 mM 4-NB, a time-dependent decrease in A_{340} was observed, indicating oxidation of NADPH to $NADP^+$ (Figure 1A). The

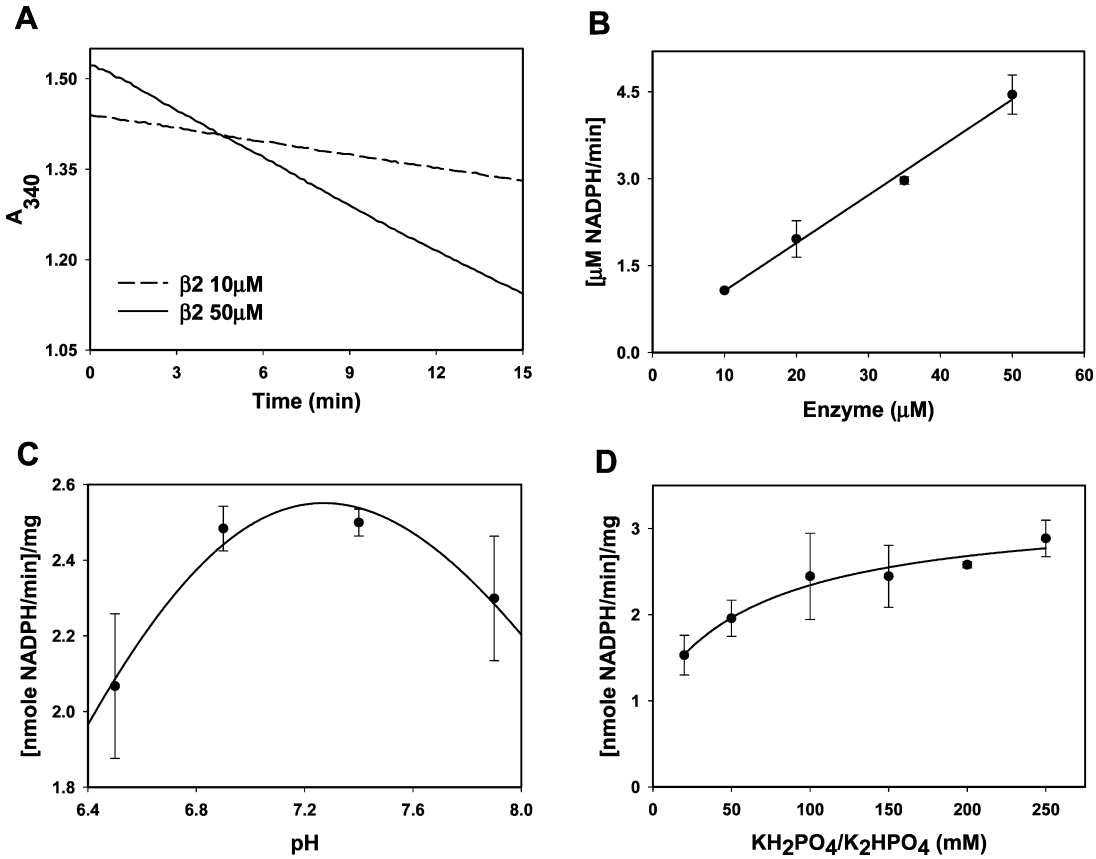

FIGURE 1: Optimal conditions for catalysis of aldehyde reduction by Kvβ2. Recombinant rat Kvβ2 was purified from *E. coli*, and the catalytic activity was measured in reaction mixtures containing 0.15 mM NADPH and 1 mM 4-nitrobenzaldehyde (4-NB). The time course of the change in absorbance at 340 nm (A_{340}) was determined at 10 (− − −) and 50 μM (—) protein in 0.2 M potassium phosphate (pH 7.4) at 37 °C (A), and the initial velocity for 10 min was calculated at different protein concentrations (B), pHs (C), and ionic strengths (D). Data are presented as means ± SEM ($n = 3$). The line in panel B is the best fit of linear equation to the data ($R^2 = 0.99$). Lines in panels C and D are the best fits of (C) a three-parameter normal logarithmic distribution ($R^2 = 0.97$) and (D) a hyperbolic ($R^2 = 0.96$) function [$y = y_0 + ax/(b + x)$] to the data.

loss of absorbance was linear for the first 10 min. The linear portion of the progress curve was used for all initial velocity measurements. The initial rate of NADPH reduction showed an increase with an increase in protein concentration (Figure 1B), indicating that the reaction was dependent on Kvβ2 and not a spurious outcome of reaction conditions. No saturation of the reaction rate was observed when the protein concentration was increased from 10 to 50 μM. Hence, in all future experiments, a protein concentration of 15−25 μM was used.

To optimize activity assays, the pH dependence of the reaction was investigated. When the enzyme activity was measured in reaction mixtures at pH 6.5−7.9, maximal activity was observed between pH 7.2 and 7.4. The enzyme activity declined at pH >7.5 or <6.5, and the pH dependence conformed to a bell-shaped curve (Figure 1C). In all subsequent measurements, a pH of 7.4 was used. Next, using a pH of 7.4, the ionic dependence of catalysis was measured. The catalytic activity of the protein was insensitive to changes in ionic strength, when the concentration of phosphate in the reaction mixture was varied between 0.1 and 0.25 M; however, a significant decrease in enzyme activity was observed at phosphate concentrations of <50 mM (Figure 1D). At 0.15 M potassium phosphate (pH 7.4), the maximal activity was ~2.5 milliunits/mg of protein, and the turnover number was between 0.08 and 0.3 min^{-1}. Under conditions optimal for NADPH oxidation, no oxidation of NADH was observed (data not shown). Moreover, inclusion of oxidized cofactor $NADP^+$ (40 μM) or the reduced product *p*-nitrobenzyl alcohol (40 μM) did not influence the initial velocity of the reaction with 4-NB, suggesting that neither product inhibition nor reverse reaction occurs to an appreciable extent during initial velocity measurements. Collectively, these data provide optimal values of protein concentration, pH, and ionic strength for the assessment of Kvβ catalysis and are consistent with the view that Kvβ2 is an enzymatically active protein that preferentially catalyzes aldehyde reduction. These results also show that the catalytic reduction of aldehydes by Kvβ2 is specific for NADPH and is not limited or affected by product inhibition.

To establish the specificity of catalysis, a site-directed Kvβ2 mutant was generated in which Tyr-90 was replaced with phenylalanine. Although previous studies show that D85N and K118M substitutions decrease the level of Kvβ2-mediated reduction of 4-CB, neither of these residues acts as an acid−base catalyst and could indirectly affect reduction by preventing substrate or NADPH binding (*18*). The residue corresponding to Tyr-90, on the other hand, is widely accepted to be a direct participant in acid−base catalysis, and substitution of this residue with phenylalanine abolishes catalytic activity in other AKRs (*21, 30, 31*). The absorbance spectrum of purified Kvβ2 Y90F was similar to that of the wild-type (WT) protein, with absorbance peaks at 275 and 360 nm (Figure 2A), indicating that the mutant protein remains tightly bound to NADPH. To quantitatively deter-

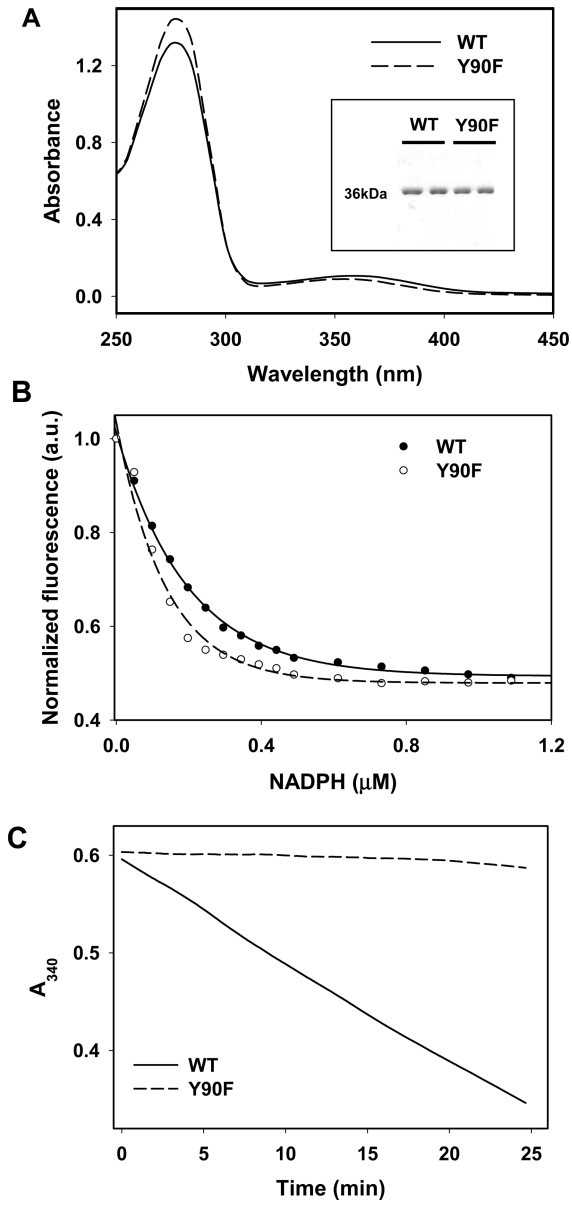

FIGURE 2: Cofactor binding and catalytic activity of Kvβ2 Y90F. (A) Absorbance spectra of WT (—) and Y90F (– – –) Kvβ2 purified from bacteria. Peak absorbance was observed at 275 nm with a shoulder at 360 nm indicating NADPH bound to the protein. The inset shows SDS−PAGE of purified WT and Y90F Kvβ2 protein. (B) NADPH-dependent changes in the fluorescence of WT (●) and Y90F (○) Kvβ2 (15 μg) measured in 0.2 M potassium phosphate (pH 7.4) using an excitation wavelength of 280 nm and an emission wavelength of 340 nm. Data are shown as discrete points, and curves are best fits of eq 1 to the data ($R^2 = 0.98$ for WT and 0.95 for Y90F). Changes in fluorescence were normalized to the initial fluorescence of the protein. (C) Time-dependent changes in absorbance at 340 nm in a reaction mixture containing 0.15 mM NADPH, 1 mM 4-nitrobenzaldehyde, and WT (—) or Y90F (– – –) Kvβ2.

mine whether the Y90F mutation affects NADPH binding, K_d^{NADPH} of the WT and mutant proteins was determined by fluorometric titrations. As shown in Figure 2B, addition of different concentrations of NADPH led to a similar decrease in the fluorescence of WT and Y90F Kvβ2. The K_d^{NADPH} for Kvβ2 WT was 0.2 ± 0.005 μM, which is similar to that determined for Kvβ2 Y90F (0.13 ± 0.011 μM), indicating that substitution of Tyr-90 with Phe does not significantly alter NADPH binding (Table 1). Nevertheless, the catalytic activity of the protein was profoundly affected. As shown in Figure 2C, significant NADPH oxidation by 4-NB was observed with the WT protein, whereas NADPH oxidation by Kvβ2 Y90F was near background levels. The turnover rate of WT Kvβ2 with 4-NB was reduced from 0.12 to 0.009 min^{-1} by the Y90F mutation (Table 1). From these results, we conclude that the aldehyde reductase activity of Kvβ2 is inherent to the protein and could not be ascribed to a contaminating protein. Moreover, the catalytic activity of the protein appears to be due to acid−base catalysis provided by Tyr-90, which corresponds to the proton donor identified in other AKRs.

Table 1: Specific Activity and NADPH Binding of WT and Y90F Kvβ2[a]

	K_d^{NADPH} (μM)	specific activity (min^{-1}) 4-nitroacetophenone (1 mM)	4-nitrobenzaldehyde (1 mM)
Kvβ2 WT	0.2 ± 0.005	0.118 ± 0.02	0.050 ± 0.008
Kvβ2 Y90F	0.13 ± 0.011	0.009 ± 0.002[b]	0.006 ± 0.003[b]

[a] Values of K_d^{NADPH} and specific activity represent means of three independent measurements. [b] $P < 0.05$ vs WT.

Substrate Specificity. To determine whether Kvβ reductase activity is limited to aldehydes or whether ketone compounds are also reduced, the enzyme activity with a series of acetophenones was measured. Of the several acetophenones tested, only 4-nitroacetophenone (4-NAP) exhibited appreciable activity. The catalytic efficiency (k_{cat}/K_m) of the protein with 4-NAP (0.46 min^{-1} mM^{-1}) was similar to that observed with 4-NB (0.59 min^{-1} mM^{-1}), indicating that Kvβ2 catalyzes the reduction of ketones as well as aldehydes. The protein also exhibited high catalytic activity with 9,10-phenanthrenequinone ($K_m = 0.24 \pm 0.14$ mM, $k_{cat} = 0.19 \pm 0.07$ min^{-1}, and $k_{cat}/K_m = 0.79$) and the endogenous carbonyl methylglyoxal ($K_m = 12 \pm 1.0$ mM, $k_{cat} = 0.32 \pm 0.04$ min^{-1}, and $k_{cat}/K_m = 0.03$). Measurable catalytic activity was also detected with several other carbonyls (Table 2) such as 4-oxo-*trans*-2-nonenal, phenylglyoxal, succinic semialdehyde, and the phospholipid aldehyde 1-palmitoyl-2-oxovaleroylphosphatidylcholine (POVPC). Low activity and poor affinity of the protein for these carbonyls, however, precluded accurate estimates of kinetic constants. Several other compounds which are generally good substrates for AKR enzymes were also tested. These include DL-glyceraldehyde, glucose, xylose, D-glucuronic acid, D-fructose, 5α-androstene 3α,17β-diol, and cortisone. We found little or no activity with these compounds under conditions optimal for other substrates. From these data, we conclude that Kvβ2 reduces both aldehydes and ketones with equal affinity.

To establish whether Kvβ2 catalysis results in the appearance of a reduced alcohol product, the protein was incubated with POVPC, which is a good substrate of AKR1B1, and other related AKRs (*32*). ESI^+/MS analysis of POVPC revealed a predominant ion at *m/z* 594.6 (Figure 3A). To examine reduction, the phospholipid aldehyde was incubated with 35 μM Kvβ2 for 180 min, after which the phospholipid was extracted using the Bligh and Dryer (*24*) procedure and re-analyzed by mass spectrometry. The phospholipid mixture recovered after incubation with Kvβ2 showed the appearance of an additional ion at *m/z* 596.4, consistent with reduction of POVPC to PHVPC. The total conversion of POVPC to PHVPC was 18 ± 2% ($n = 4$), which corresponds to the

Table 2: Kvβ2 Specific Activity with Biological Carbonyls

	Substrate	Structure	Specific activity (min^{-1})
1.	Phenylglyoxal (100 μM)	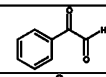	0.014 ± 0.0006
2.	Methylglyoxal (12 mM)	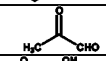	0.32 ± 0.04
3.	3-deoxyglucosone (5 mM)	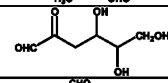	0.039 ± 0.01
4.	2-carboxybenzaldehyde (10 mM)	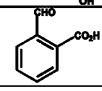	0.010 ± 0.005
5.	Acrolein (100 μM)	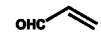	0.010 ± 0.003
6.	4-oxo-nonenal (100 μM)	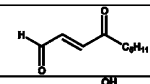	0.028 ± 0.004
7.	4-hydroxy-nonenal (100 μM)	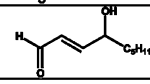	–[a]
8.	Succinic semialdehyde (25 mM)	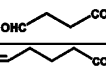	0.011 ± 0.004
9.	12-oxoETE (10 μM)	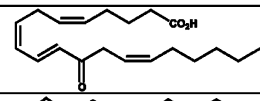	0.044 ± 0.007
10.	PGJ_2 (100 μM)	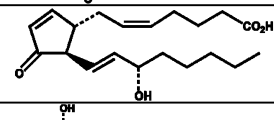	0.086 ± 0.019
11.	PGD_2 (100 μM)	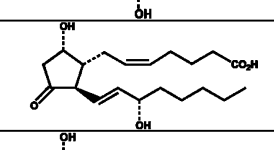	–[a]
12.	$PGF_{2\alpha}$ (100 μM)	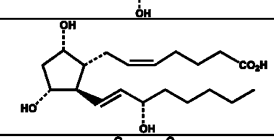	–[a]
13.	9, 10 Phenanthrenequinone (200 μM)	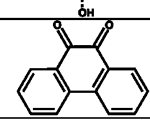	0.19 ± 0.07
14.	POVPC (100 μM)	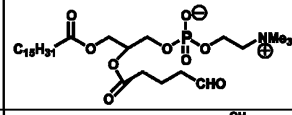	0.078 ± 0.016
15.	5α-androstan-17β-ol-3-one (100 μM)	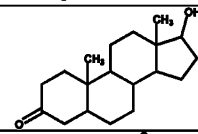	–[a]
16.	Cortisone (100 μM)	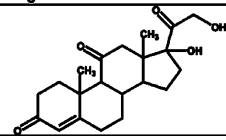	–[a]

[a] Activity of <2-fold over the background.

amount of NADPH oxidized. These observations confirm the AKR nature of the Kvβ2 active site and substantiate its catalytic activity, leading to the generation of a reduced product.

Because Kvβ2 can reduce both aldehydes and ketones, we asked which of these groups is preferentially reduced by Kvβ2 in a keto aldehyde. To test this, the protein was incubated with 4-ONE, which contains a keto group at C-4 and an aldehyde at C-1. As shown in Scheme 1, reduction of this compound at C-1 should result in the formation of 4-oxononenol, whereas reduction at C-4 should form 4-HNE. Further reduction of 4-HNE and 4-oxononenol would lead to formation of DHN. The Kvβ-derived product of 4-ONE was first analyzed by HPLC. As shown in Figure 4, an appropriate separation protocol was developed in which the retention times of 4-HNE, DHN, 4-ONE, and 4-oxononenol were measurably different. Incubation with Kvβ2 shifted the retention time of 4-ONE from 53 to 37 min, which corresponds to the retention time of 4-oxononenol. No products eluted with a retention time corresponding to that of 4-HNE or DHN, indicating that Kvβ2 reduces 4-ONE to 4-oxononenol. To further confirm the structural identity of the product, the Kvβ2-derived peak at 37 min was derivatized and analyzed by GC−MS. On GC, the product exhibited a

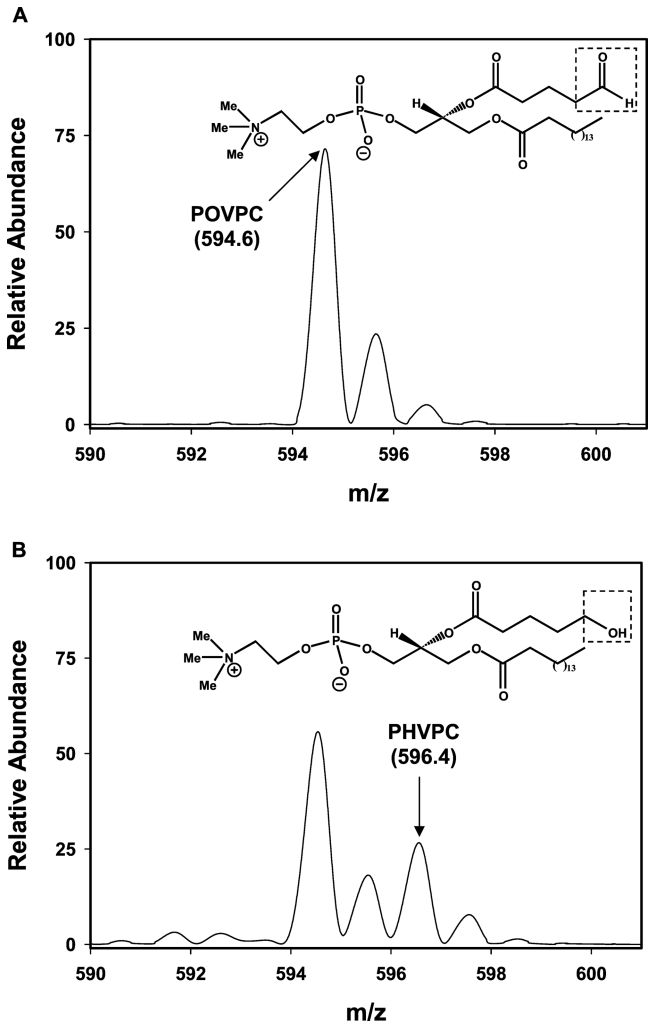

FIGURE 3: Kvβ2-catalyzed reduction of phospholipid aldehyde. Electrospray mass spectra of 1-palmitoyl-2-oxovaleroylphosphatidylcholine (POVPC) incubated without (A) and with (B) Kvβ2. The formation of the reduced product, 1-palmitoyl-2-oxovaleroylphosphatidylcholine (PHVPC), is evident in the appearance of a new ion at *m/z* 596.4. For reduction, POVPC (80 μM) was incubated without or with Kvβ2 (35 μM) and NADPH (0.15 mM) for 180 min at 37 °C. The 2 Da increase in *m/z* was assigned to an alcohol generated by the reduction of the aldehyde at the *sn*-2 position (as indicated).

retention time of 8.06, which was identical to that of reagent 4-oxononenol. On the mass spectrum of the product (Figure 4C), the derivatized molecular ion at *m/z* 228 (M) was identified, along with major fragments at *m/z* 213 ($M - CH_3$), 157 ($M - C_5H_{11}$), and 129 ($M - C_6H_{11}O_1$). This fragmentation pattern corresponds to 4-oxononenol, but not 4-HNE, 4-ONE, or DHN (data not shown), indicating that the keto group at the C-4 position remains unreduced whereas the aldehyde group at the C-1 position is reduced, leading to the formation of 4-oxo-2-nonenol. These data suggest that Kvβ prefers aldehydes to ketones and that carbonyls with a high electron density at oxygen (e.g., C-1 of 4-ONE) are reduced more efficiently than less polarized carbonyls (e.g., C-4 of 4-ONE or C-1 of 4-HNE).

Reaction Sequence. To determine the reaction sequence of the catalytic cycle, the initial velocity of the reaction was measured at different 4-NB and NADPH concentrations. For these experiments, 4-NB was chosen as the model substrate because of all the carbonyls examined, the highest k_{cat}/K_m values and low K_m values were observed with 4-NB. Double-reciprocal plots of initial velocity versus substrate concentration were linear and showed no signs of product or substrate inhibition. Double-reciprocal plots at different NADPH concentrations conformed to a pattern of straight lines intersecting at the ordinate (Figure 5). This pattern is consistent with a rapid equilibrium ordered kinetic mechanism in which NADPH binds first to the enzyme followed by the carbonyl substrate (Scheme 2). To determine kinetic constants, the following relationship was used:

$$v = \frac{V_M AB}{K_{ia}K_b + K_b A + AB} \quad (6)$$

where A is the concentration of NADPH, B is the concentration of 4-NB, V_M is V_{max}, K_b is the Michaelis constant for 4-NB, and K_{ia} is the binding constant of NADPH. The best fit of eq 6 to the data yielded the following values: $K_{ia} = 107 \pm 33$ μM, $K_b = 490 \pm 119$ μM, and k_{cat} (V_M/E_t) $= 0.15 \pm 0.015$ min^{-1}. When the equation for a steady-state ordered mechanism containing the term K_aB in the denominator of eq 6 was fitted to the data, an undefined K_a was obtained. A replot of slopes (K_b/V_m apparent) (determined from Figure 5) versus 1/NADPH was linear with a slope of K_bK_{ia}/V_m and an intercept on the ordinate axis of K_b/V_m. The intercept on the 1/NADPH axis was equal to $-1/K_{ia}$. Values obtained from each curve separately (slope replot; Figure 5, inset) are similar to those determined by global analysis (i.e., by fitting eq 6 to the data). These data confirm that Kvβ2 follows a rapid equilibrium ordered scheme in which NADPH binding precedes substrate binding (Scheme 2).

Kinetic Isotope Effects. To improve our understanding of the mechanism of Kvβ2 catalysis in greater detail, we investigated the rate-determining step. For this, the primary kinetic isotope effects were determined by using NADPH and NADPD as cofactors. NADPH and NADPD were synthesized as described in Experimental Procedures, and the initial velocity was measured at different concentrations of the aldehyde substrate. In the first series of experiments, Kvβ2 activity was measured using 4-NB or 4-NAP as the variable substrate. Both eqs 4 and 5 were used to fit the data obtained (Figure 6). Equation 5, however, gave a better fit to the data than eq 4 as determined by F values and the standard errors in the values of the kinetic constants. The best-fit values of kinetic constants obtained from eq 5 are listed in Table 3. Similar values of kinetic isotope effects were obtained with either 4-NB or 4-NAP as the varied substrate (Table 3). High primary kinetic isotope effect values indicate that the chemical step is rate-limiting in Kvβ2-catalyzed reduction. The lack of an isotope effect on K_b suggests that K_m is not a true steady-state kinetic parameter, but a dissociation constant for aldehyde binding to the E−NADPH binary complex. The reverse reaction, i.e., oxidation of 4-nitrobenzyl alcohol by $NADP^+$, was also investigated. However, with 4-nitrobenzyl alcohol as the substrate, no measurable activity under multiple-turnover conditions was detected. This precluded determination of a Haldane relationship and calculation of several microscopic constants, including k_{-3}, which is the rate constant for alcohol oxidation (Scheme 2).

Single-Turnover Measurements. Transient kinetic measurements, such as single turnover, allow determination of some of the microscopic rate constants associated with

Scheme 1: Potential Products of 4-Oxo-2-nonenal (4-ONE) Reduction[a]

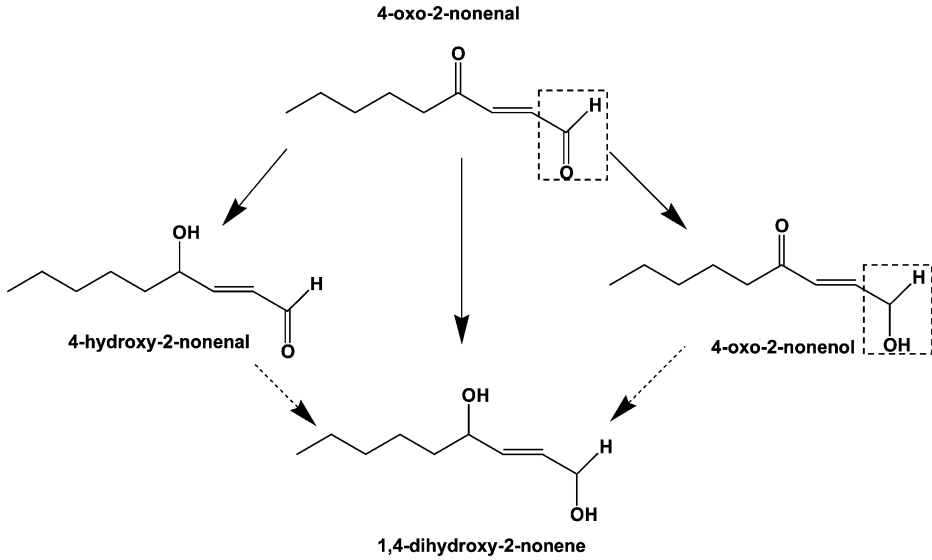

[a] Reduction of 4-oxo-2-nonenal at C-1 aldehyde would lead to the formation of 4-oxo-2-nonenol, whereas reduction of the C-4 keto group should yield 4-hydroxy-2-nonenal (4-HNE). Additional reduction of 4-HNE or 4-oxo-2-nonenol would form 1,4-dihydroxy-2-nonenal (DHN). Note that reduction in the presence of Kvβ2 led to the appearance of only 4-oxo-2-nonenol. No 4-HNE or DHN formation was observed (see Figure 4). Reduction of the C-1 aldehyde to an alcohol is indicated by a dashed box.

catalysis. Kvβ2 binds tightly to NADPH and forms a binary complex. Free NADPH in solution absorbs at 340 nm, whereas binding to the β2 subunit causes a red shift of this peak to 360 nm. Hence, for single-turnover experiments, we monitored changes in absorbance at 360 nm to measure the activity of the β2−NADPH binary complex with 4-NB.

To measure isotope effects under single-turnover conditions, the Kvβ2 protein was preloaded with NADPD. Because Kvβ2 purified from bacteria is tightly bound to NADPH (Figure 7A), NADPH bound to Kvβ2 was first oxidized to $NADP^+$ in a single-turnover reaction using 4-NB as the substrate. As shown in Figure 7A, incubation with 4-NB led to a progressive decrease in A_{360}, indicating that all of the NADPH bound to the protein was oxidized to $NADP^+$. Unutilized 4-NB and 4-nitrobenzyl alcohol generated from the reaction were removed by equilibrium dialysis. The protein was reloaded with either NADPH or NADPD by dialysis with either of these cofactors. This led to an increase in absorbance at 360 nm, indicating that $NADP^+$ bound to the protein was completely replaced by NADPH or NADPD. Analysis of the absorbance at 275 and 360 nm using an extinction coefficient of 60880 M^{-1} cm^{-1} for the protein and 6200 M^{-1} cm^{-1} for NADPH indicated that approximately 90−100% of the protein was saturated with NADPH/D (Figure 7A). These preparations were then used for subsequent kinetic isotope studies under single-turnover conditions.

Absorbance at 360 nm decreased with time upon addition of 4-NB (0.2−2 mM) to the NADPH- or NADPD-loaded enzyme (Figure 7B,C). Experimental time courses for NADPH/D oxidation were best described by a single-exponential function. Values of k_{trans} increased linearly with 4-NB concentration and showed no significant saturation within the concentration range of 4-NB that could be practically achieved (Figure 7D). From these experiments, a kinetic isotope effect of 3.13 ± 0.2 was obtained (Table 3), indicating that the chemical step is rate-limiting under single-turnover conditions.

Structure−Activity Relationship. To improve our understanding of the catalytic mechanism, Hammett plots with catalytic efficiencies (k_{cat}/K_m) and turnover numbers (k_{cat}) were generated with a series of para-substituted benzaldehydes (Figure 8A,B). A plot of log k_{cat}/K_m versus σ^+ displayed a linear relationship (Figure 8A), suggesting that the reaction mechanism does not change within this series and that substituent effects was primarily electronic in nature. A Hammett plot with k_{cat}/K_m showed a positive ρ coefficient, the value (1.95 ± 0.36) of which is similar to that reported for other AKRs (*22, 29*). This fit was only marginally improved by incorporating the hydrophobicity or the steric constants (Table 1 of the Supporting Information), indicating that these characteristics make only minor contributions to benzaldehyde binding. A plot of k_{cat} versus σ^+ gave a slope of 0.04 ± 0.02 (Figure 8B). Among the series that were tested, the only exception was 4-NB. Reasons for the anomalous behavior of 4-NB are unclear but may relate to specific interaction of the nitro group with the active site residues of the protein. Log K_m displayed a linear inverse relationship with σ^+ with a correlation coefficient (ρ) of −1.85 ± 0.52 (Figure 8C), and no significant contribution of steric or hydrophobic features of the benzaldehydes was evident (Table 1 of the Supporting Information).

DISCUSSION

The β-subunits of voltage-gated (Kv) potassium channels belong to the AKR superfamily of enzymes (*13*). The sequences of these proteins are 20−26% identical with those of other members of the family, and the architecture of their active site resembles that of other AKR oxidoreductases (*12*). Nevertheless, their catalytic properties are largely unknown. We, therefore, studied the substrate specificity and kinetic behavior of Kvβ2 to identify features of catalysis that are

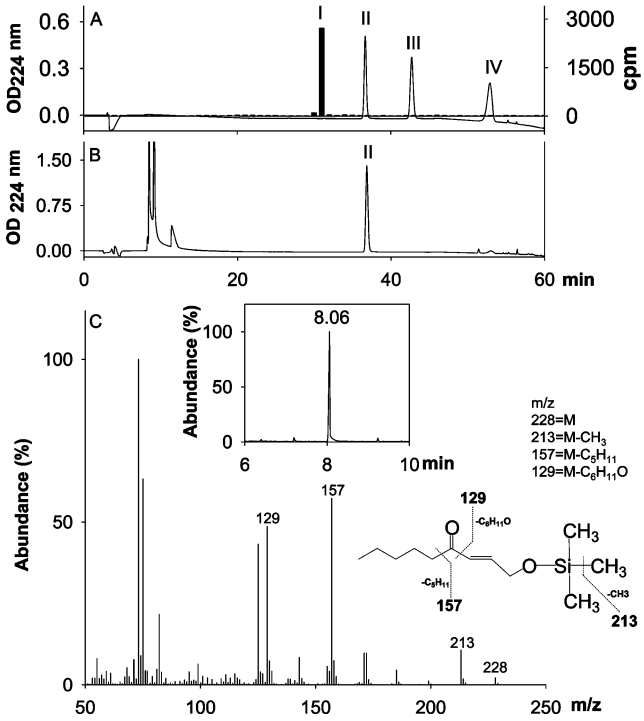

FIGURE 4: Identification of the product generated by the reduction of 4-oxo-2-nonenal (4-ONE) by Kvβ2. Panel A shows the separation of reagent [^{3}H]-1,4-dihydroxynonenol (DHN, 3000 cpm), 4-oxo-2-nonenol, 4-hydroxy-2-nonenal (4-HNE), and 4-ONE, 40 nmol each on a ODS C_{18} reverse phase HPLC column. The *y*-axis on the right side shows the radioactivity profile of [^{3}H]DHN, whereas the *y*-axis on the left side shows OD_{224}. Peaks I−IV eluting with retention times of 31, 37, 43, and 53 min are due to reagent DHN (I), 4-oxo-2-nonenol (II), 4-HNE (III), and 4-ONE (IV), respectively. Panel B shows the HPLC separation of the 4-ONE product generated by Kvβ2-catalyzed reduction. Reagent 4-ONE (100 nmol) was incubated with 0.6 mg of Kvβ2 and 0.3 mM NADPH in 0.2 M potassium phosphate for 2 h at 37 °C, and the product was separated via HPLC. The inset of panel C shows a representative gas chromatogram of derivatized peak II (from panel B), eluting at 8.06 min, and shows the electron impact ionization mass spectrum of the siliated metabolite of the GC peak eluting at 8.06 min. The ion at *m/z* 228 represents the moleclular ion (M) of 4-oxo-2-nonenol. Ions at *m/z* 213, 157, and 129 correspond to M − CH_3, M − C_5H_{11}, and M − $C_6H_{11}O$ fragments of 4-oxo-2-nonenol, respectively.

unique to Kvβ proteins and those that they share with other AKRs. Our results show that Kvβ2 displays significant enzyme activity and that it utilizes NADPH to catalyze the reduction of both aldehydes and ketones. As expected for an enzyme reaction, the rate of reduction was increased with an increase in protein and substrate concentration; the reaction showed distinct pH and ionic strength dependence, and the initial velocity was saturated at high substrate concentrations. Importantly, catalysis, but not NAPDH binding, was prevented by substituting tyrosine 90 with phenylalanine, indicating that, as in other AKRs (*21, 30, 31*), in Kvβ2 this residue participates in general acid−base catalysis and that carbonyl reduction is not due to contamination by other proteins in the preparation or a direct covalent reaction with NADPH, but that it is a controlled conversion catalyzed at the Kvβ2 active site.

Substrate specificity studies show that the protein was active with several aldehydes and ketones. The highest activity was observed with aromatic substrates. Comparable activity was observed with benzaldehydes and acetophenone as well as 9,10-phenanthroquinone. Most AKRs display high catalytic activity with 4-nitrobenzaldehyde [$K_m = 2$ μM (AKR1B1) (*33*) or 3 mM (AKR7A2) (*34*)] and methylglyoxal [$K_m = 8$ μM (AKR1B1) or 1.2 mM (AKR1A1) (*35*)], with k_{cat} ranging from 24 to 360 min^{-1} (*33, 36*). 4-Nitroacetophenone and 9,10-phenanthrenequinone are typical model substrates for the AKR1C family members, which have substantial catalytic activity with ketone as well as aldehyde compounds. These enzymes possess lower k_{cat} values (2−190 min^{-1}); however, K_m values typically lie in the low micromolar range (1−200 μM) (*31, 34*). Several physiological aldehydes such as lipid peroxidation products 4-HNE and POVPC are specific substrates for the AKR1B enzymes (*32, 37*). Our results show that Kvβ catalyzes the reduction of a similar range of aldehydes and ketones with K_m values in the range observed with other AKRs. On the basis of substrate specificity showing that it could catalyze the reduction of both aldehydes and ketones, we propose that Kvβ2 should be considered a general AKR rather than an aldehyde or a ketone specific reductase. Nevertheless, when both aldehyde and ketone groups were presented to the enzyme in the same substrate (e.g., in 4-ONE), the enzyme reduced the aldehyde, indicating that it prefers more electronegative carbonyls.

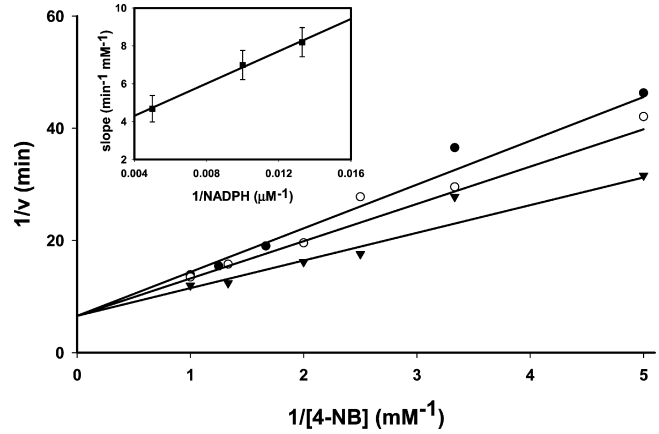

FIGURE 5: Initial velocity profile of reduction of aldehyde by Kvβ2. Double-reciprocal plots of initial velocity were derived by measuring the rate of change of absorbance at 340 nm at different concentrations of 4-nitrobenzaldehyde at 75 (●), 100 (○), and 200 μM NADPH (▼). Lines represent the best fit of eq 6 to the data ($R^2 = 0.97$). The inset shows a replot of individual slopes of the double-reciprocal plot vs 1/NADPH.

Scheme 2: Catalytic Cycle for NADPH-Dependent Carbonyl Reduction by Kvβ2[a]

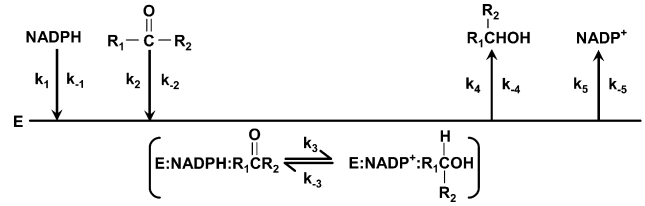

[a] Sequential binding of the protein to NADPH and the carbonyl substrate results in the formation of a ternary complex in which the carbonyl is reduced to its corresponding alcohol. The release of products is also shown to be ordered. The microscopic rate constants for each reaction step in the forward and reverse directions are indicated as k_n and k_{-n}, respectively.

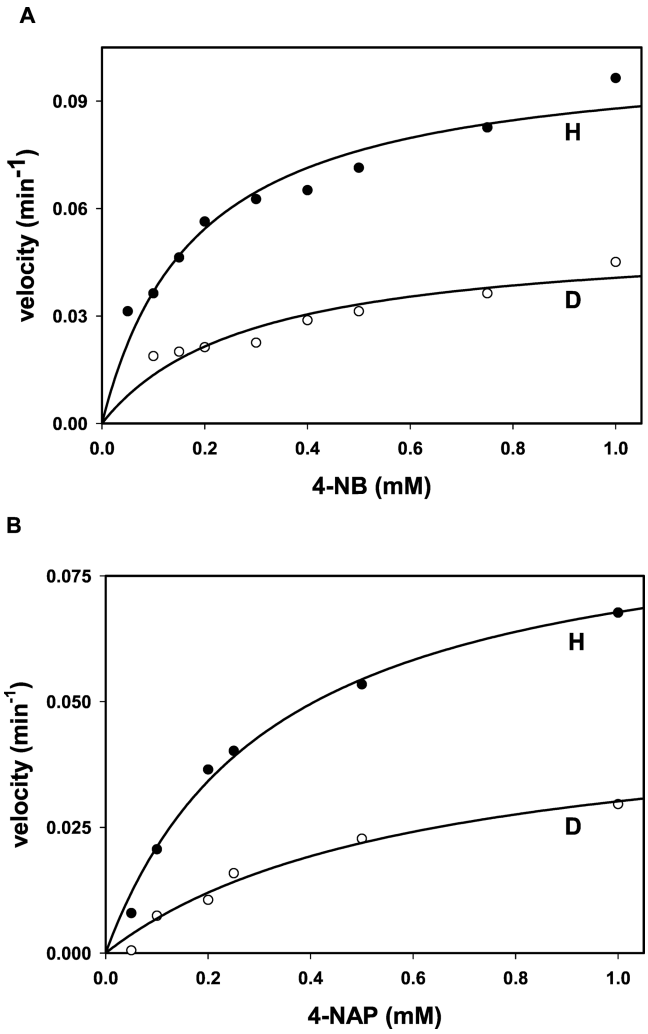

FIGURE 6: Primary deuterium kinetic isotope effects on Kvβ2-catalyzed aldehyde reduction. Initial velocity plots of the reaction at different concentrations of 4-nitrobenzaldehyde (A) and 4-nitroacetophenone (B) with 0.15 mM NADPH or NADPD as indicated. For each measurement, the Kvβ2 protein was mixed with either NADPH or NADPD (0.15 mM) and the reaction was initiated by the addition of the substrate. Time-dependent changes in absorbance (multiple-turnover mode) were measured. Values of initial velocity are normalized to Kvβ2 concentration. Data are shown as discrete points, and curves are best fits of eq 5 to the data ($R^2 = 0.99$ for 4-NB and 0.97 for 4-NAP).

The physiological substrate of Kvβ2 remains unknown. The protein, however, exhibited high catalytic activity with several carbonyls that are generated endogenously from enzymatic and nonenzymatic oxidation of lipids. High activity was observed with two enzymatically generated carbonyls, 12-oxo-ETE and PGJ_2. 12-oxo-ETE is a leukotriene B4 receptor agonist (*38*) and is derived from the oxidation of arachidonic acid by 12-lipoxygenase (*39*), whereas PGJ_2 is a precursor of 15-deoxy Δ12,14-PGJ_2, which is thought to be a natural ligand of the peroxisome proliferator-activated receptor (PPAR-γ) (*40*). Carbonyl compounds generated from nonenzymatic oxidation of phospholipids such as 4-HNE, 4-ONE, and POVPC were also reduced by Kvβ2. These aldehydes are reactive chemicals, and they affect a variety of signaling pathways, leading to changes in vasodilation (*41*), myocyte excitability (*42*), and cell adhesion (*43*). Steroid-based natural carbonyl compounds such as 5α-androstene-3,17-dione, 4-androstene-3,17-dione, and cortisone, on the other hand, were minimally reduced under conditions that were optimal for the reduction of other carbonyls. Whether any of these carbonyls are reduced by the protein in vivo remains unclear. Nonetheless, the preference of Kvβ2 for hydrophobic aldehydes raises the possibility that the function of this protein is related to the reduction of membrane-derived oxidized lipids.

Our kinetic analyses suggest that Kvβ2 follows rapid equilibrium kinetics in which the bond-breaking step is rate-limiting (Scheme 2). This scheme is consistent with the lack of an isotope effect on K_m and the convergence of double-reciprocal initial velocity plots at different substrate concentrations on the ordinate. This plot also indicates that the enzyme follows an obligate ordered reaction sequence, with the coenzyme binding first. Significant primary kinetic isotope effects were observed on k_{cat}, indicating that chemistry is rate-limiting. Single and multiple turnovers displayed similar isotope effects (Table 3), although the slightly higher values for single (3.13) versus multiple (2.07) turnovers may be due to kinetic steps that contribute to multiple-turnover, but not single-turnover, reactions. These steps include those leading to NADPH binding (k_1, Scheme 2) or $NADP^+$ release (k_5). They appear to be nearly as slow as the bond-breaking step (k_3) and could thus contribute to the rate of the overall reaction cycle. The value of the microscopic rate constant for the chemical step (k_3) can be estimated from the following relationship:

$$k_3 = k_{cat}({}^{D}k_3 - 1)/({}^{D}k_{cat} - 1) \quad (7)$$

If we assume that the ${}^{D}k_3$ value of 6.5, as calculated from NADPH-dependent reduction of D-xylose by AKR1B1 (*44*) and consistent with the kinetics of *Candida tenuis* xylose reductase (*29*), then calculations using eq 7 show that $k_3 = 0.82 \pm 0.15$ min^{-1} for 4-NB and 0.73 ± 0.05 min^{-1} for 4-NAP. However, if we use a value of 3.1 estimated by Jin et al. for the intrinsic isotope effect on the AKR1C2-catalyzed reduction of 5α-DHT by NADPH (*45*), k_3 for 4-NB is 0.31 ± 0.06 min^{-1}. Both these values are in agreement with the estimate for k_3 obtained from our single-turnover experiments. Fitting of multiple single-turnover traces obtained with various 4-NB concentrations (Figure 6) using Dynafit predicts that k_3 is between 0.3 and 0.8 min^{-1}. This prediction suggests that 20−50% of the overall rate limitation is due to the hydride transfer step with the remainder contributed by $NADP^+$ or product release. A slow release of $NADP^+$ has been identified to be the rate-limiting step in the AKR1B1-catalyzed aldehyde reduction (*44*) and is believed to be due to the slow movement of the NADPH binding loop (*44, 46*). This possibility is consistent with the crystal structure of Kvβ2, which shows that the cofactor is held tightly at the active site (*12*). Thus, $NADP^+$ release, which requires extensive conformational rearrangement, could contribute to the inequality of isotope effects between single- and multiple-turnover reactions and, by implication, to the overall rate of the catalytic cycle.

Our data exclude cooperative or allosteric effects on catalysis and are consistent with our previous work showing a lack of cooperativity in NADPH or $NADP^+$ binding to Kvβ2 (*14*). Native Kvβ proteins are, however, arranged as a tetramer around the T1 domain of Kvα (*47*), and Kvβ2 purified from bacteria (used for the kinetic experiments

Table 3: Kinetic Constants and Primary Kinetic Isotope Effects (KIEs) on Kvβ2-Mediated Carbonyl Reduction[a]

substrate	K_m (μM)	k_{cat} (min^{-1})	k_{cat}/K_m (mM^{-1} min^{-1})	KIE
4-nitroacetophenone	209 ± 49	0.092 ± 0.006	0.46 ± 0.09	1.69 ± 0.1
4-nitrobenzaldehyde	283 ± 31	0.16 ± 0.030	0.59 ± 0.17	2.07 ± 0.4
4-nitrobenzaldehyde[b]	–[c]	–[c]	–[c]	3.13 ± 0.2

[a] The value of each parameter is a representative of two to five separate determinations using different preparations of the protein. For each determination, the initial velocity was measured at six to nine different concentrations of the substrate. [b] Data from single-turnover experiments. [c] Not determined.

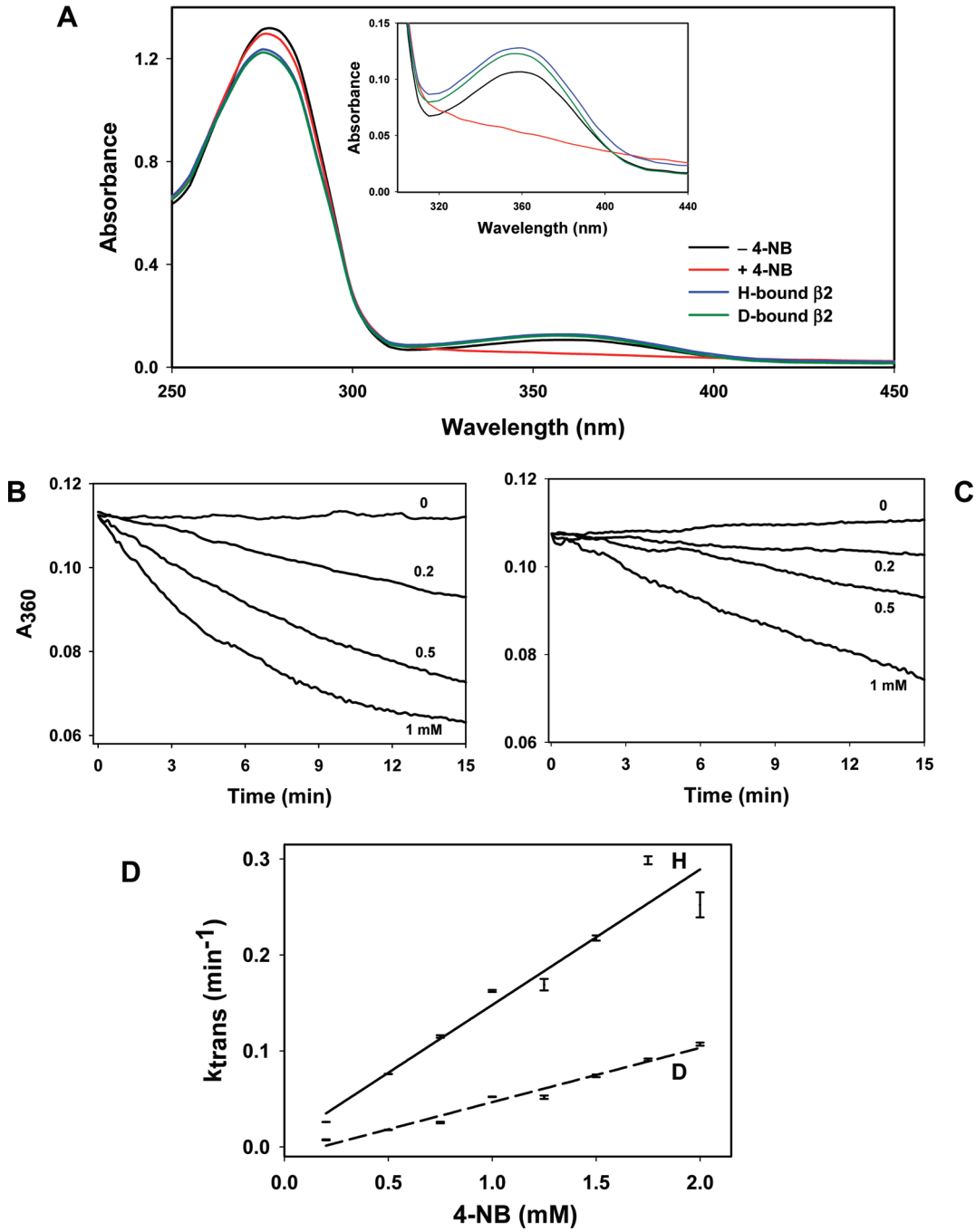

FIGURE 7: Kinetic isotope effects on single-turnover reactions of Kvβ2. (A) Replacement of protein-bound NADPH with NADPD. The NADPH bound to Kvβ2 (black) was oxidized by incubating the protein with 1 mM 4-nitrobenzaldehyde. This led to a progressive decline in absorbance of the protein at 360 nm (inset, red line), indicating oxidation of NADPH to $NADP^+$. The reaction mixture was then dialyzed for 16−20 h at 4 °C against 0.2 M potassium phosphate (pH 7.4). The protein was then incubated with reagent NADPH or NADPD for 30 min at 4 °C and dialyzed for 16−20 h. Reloading with NADPH (blue) or NADPD (green) led to an increase in A_{360}, indicating reformation of the protein−nucleotide binary complex; Time-dependent decrease in A_{360} of NADPH-bound (B) and NADPD-bound (C) Kvβ2 incubated with the indicated concentrations of 4-NB. (D) Values of the pseudo-first-order rate constant (k_{trans}), obtained by fitting a single-exponential equation to the progress curve data shown in panels B and C, plotted as function of 4-NB concentration. Data are shown as discrete points ± SEM, and lines are best fits of eq 5 to the data ($R^2 = 0.96$) [(—) NADPH and (– – –) NADPD].

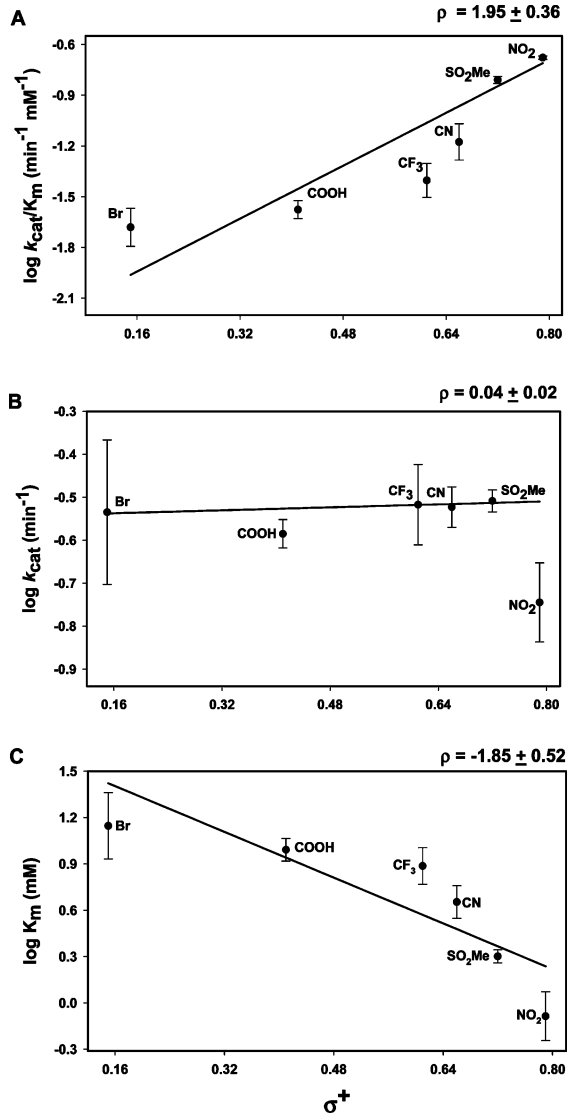

FIGURE 8: Structure−activity relationships for Kvβ2-mediated reduction of substituted benzaldehydes. Relationships between (A) log k_{cat}/K_m, (B) log k_{cat}, and (C) log K_m of para-substituted benzaldehydes and the Hammett constant, σ^+. The enzyme activity was determined under multiple-turnover conditions with 0.15 mM NADPH. Data are shown as discrete points, and lines are best weighted fits of a linear equation to the data ($R = 0.79-0.93$). Calculated slopes are listed at the top right corner of each panel. Results of multivariate regression analysis are listed in Table 1 of the Supporting Information.

described here) is a tetramer in solution (*14*), indicating that cooperative behavior is possible. Nevertheless, no cooperativity was observed. Perhaps in solution, as in crystal structure with T1 (*47*), the active site of Kvβ faces the solvent and is minimally affected by other β-monomers in the complex. Nonetheless, the possibility of allosteric effects in the regulation of Kv current by the β-subunits in situ cannot be ruled out.

The catalytic mechanism for carbonyl reduction by Kvβ2 appears to be similar to that observed for other AKRs. Catalytic inactivation by the Y90F mutation suggests that this residue play a similar role in Kvβ2 as it does in other AKRs (*21, 30, 48*). In addition to tyrosine (Tyr- 48 in AKR1B1), an active site histidine residue (His-110 in AKR1B1) has also been suggested to play an important role in AKR catalysis and substrate binding (*21, 30, 49*). This residue is located at the center of the hydrogen bonding network that facilitates substrate binding and polarization of the substrate carbonyl (*48, 50*). The imidazole of this histidine in AKR2B5 plays an important role in precise positioning of the carbonyl group for catalysis (*50*). Significantly, His-110 is absent in Kvβ and is replaced by an asparagine residue. This shift in charge is likely to prevent tight binding of the carbonyl at the active site and may be responsible for the low catalytic activity of Kvβ2 (0.06 to 0.2 min^{-1} versus 2 to 600 min^{-1} for other AKRs). Low catalytic rates of Kvβ2 could thus be due to lose positioning and partial charge delocalization at the carbonyl caused by the sole tyrosine phenolate residue rather than a complex between a tyrosine and histidine as in other AKRs. Indeed, replacement of His-113 in AKR2B5 with alanine causes a 600- to1000-fold decrease in the catalytic activity of the protein (*50*).

Despite the absence of an active site histidine, substrate binding to the Kvβ active site was similar to that of other AKRs. Our previous experiments with AKR1A1 show a strong dependence of k_{cat}/K_m as well as k_{cat} on variations in substituents on the aromatic ring of benzaldehyde substrate (*22*). Similar results have been reported for AKR2B5 (*29*). Indeed, the ρ value obtained from the Hammett plot of k_{cat}/K_m for Kvβ2 (1.95) was comparable to the ρ values obtained for AKR1A1 (1.95) and AKR2B5 (1.4). These data suggest that the active sites of AKRs are similar and that electron-withdrawing groups stabilize the formation of the ternary complex in the catalytic cycle of these proteins. Moreover, a negative correlation of K_m with σ^+ in Kvβ2 indicates that the binding of benzaldehydes is strongly dependent on the electron-withdrawing potential of para substituents. The ρ value for K_m of Kvβ2 (−1.85) is, however, higher than that of AKR1A1 (−0.95) (*22*), indicating that electronic features play a more important role in substrate binding to Kvβ2 (AKR6) than in AKR1A1. The importance of the electronic feature is further underscored by the observation that Kvβ2 was active with PGJ_2, which contains a carbonyl polarized by α,β-unsaturation, but not PGD_2 (Table 2), which is identical to PGJ_2 except that it lacks the conjugated system and therefore has a less polarized carbonyl. Likewise, the more electrophilic C-9 aldehyde 4-ONE was a substrate, but the less polarized 4-HNE, despite a similar structure, was not reduced. Hence, a polarized carbonyl with a partial negative charge on the oxygen appears to favor substrate binding. Furthermore, the correlation between substrate binding and σ^+ within the benzaldehyde series suggests that a negative charge develops on the substrate carbonyl during ground-state interaction, which may be indicative of the presence of a positively charged group that forms a hydrogen bond with the substrate (Scheme 3, complex 1). The identity of this group remains to be established; however, Tyr-90 is a strong possibility, and binding to this residue could increase the level of polarization of the enzyme carbonyl (Scheme 3).

In contrast to binding, the bond-breaking step (k_{cat}) was relatively insensitive to the polarizing effects of substituents. In this regard, Kvβ2 is different from AKR1A1 which gives a ρ value of 0.8 for the Hammett plot of k_{cat} (*22*). The most straightforward explanation is that in Kvβ2, the charge developed on the carbonyl in the transition state is small. Given, however, that acid−base catalysis by other AKRs

Scheme 3: Mechanism of NADPH-Dependent Carbonyl Reduction Catalyzed by Kvβ2[a]

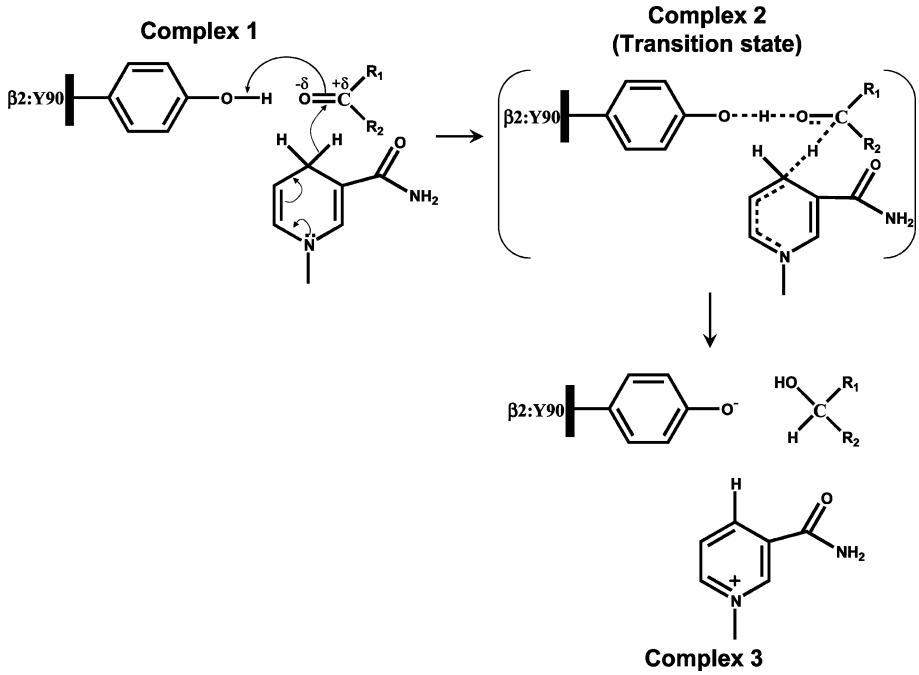

[a] In complex 1, Tyr-90 is shown poised to form a hydrogen bond with the substrate carbonyl which results in carbonyl polarization, accelerating the hydride transfer of the *pro-R* hydrogen from the nicotinamide ring of NADPH to the carbonyl carbon of the substrate. Complex 2 shows a noncharged transition state in which the polarization at the carbonyl is quenched by the transfer of a proton from the protein tyrosine and a concerted hydride transfer to the carbonyl carbon. The reduced carbonyl then dissociates from the acid−base catalyst, and a net charge develops on the oxidized cofactor and the tyrosinate anion (complex 3).

involves polarization of the substrate carbonyl, we suggest that in Kvβ the charge develops in the ground state of the carbonyl group. This polarization leads to the development of a slightly negative carbonyl O-1 and a slightly electron-deficient C-1 (Scheme 3, complex 1). During the transition state, these charges are rapidly compensated by the transfer of a proton to O-1 and the transfer of a hydride to C-1 (Scheme 3, complex 2). Because these events occur in concert, no net charge develops during the transition state. This mechanism appears to be similar to that of AKR2B5, which also shows no significant substituent effects (*29*), but differs from AKR1A1 catalysis. Substituent effects on AKR1A1 are more consistent with a stepwise hydride and proton transfer leading to the formation of a charged transition state. Overall, it appears that in Kvβ2-mediated catalysis, the lack of hydrogen bonding (due to the absence of an active site histidine) prevents stabilization of a transition state in which the carbonyl is hydrogen bonded before the proton transfer occurs. Therefore, the reaction proceeds with a concerted, rather than stepwise, hydride and proton transfer (Scheme 3, complex 2). We speculate that this mechanism may be particularly relevant to the regulation of Kvβ catalysis by membrane voltage and to the ability of Kvβ to alter Kv inactivation.

It has been suggested that the reason why Kv channels associate with auxiliary subunits possessing oxidoreductase activity is related to two possibilities (*51*). The first possibility is that the Kvβ proteins are redox sensors that couple changes in the intracellular redox state with membrane excitability. This possibility is consistent with Kvβ-dependent changes in Kv inactivation in cells subjected to hypoxia (*52*). On the basis of the high NADPH binding affinity of Kvβ and the observation that Kvβ-mediated Kv inactivation is reversed by $NADP^+$, but not NADPH, we had suggested that changes in intracellular oxygen or intermediary metabolism could affect Kv currents by altering the redox state of nucleotides bound to Kvβ (*16*). The redox state of the nucleotide bound to the protein could also be changed by catalysis, and in view of the high catalytic activity of the protein with several endogenous carbonyls, it appears likely that changes in endogenous NADPH-reducible endogenous carbonyls could regulate Kvβ activity, and in turn the inactivation, or voltage dependence, of Kv channels. Furthermore, because the dissociation constants of Kvβ for NADPH and $NADP^+$ (0.1−0.6 μM) are far below the range of physiological changes in pyridine nucleotide concentration, the protein under most conditions is likely to respond to changes in the concentration of the carbonyl substrate. Thus, any oxygen- or metabolism-dependent changes in substrate carbonyl concentration will rapidly alter the catalytic rate of Kvβ, leading to cofactor oxidation and changes in Kv channel activity (*15, 16*).

A second scenario holds that voltage-dependent changes in the Kv channel could regulate Kvβ catalysis by affecting the configuration of the Kvβ active site. We suggest that a mechanism in which catalysis is rate-limiting is ideally suited for such a voltage-sensitive oxidoreductase. Because catalysis or the rate of interconversion of the ternary complexes could be regulated by a single step (independent of cofactor or substrate concentration), voltage changes could efficiently modulate the overall rate of the reaction. Clearly, further experiments are required to fully evaluate and assess the physiological implications of the kinetic behavior of Kvβ proteins.

ACKNOWLEDGMENT

We thank Yuting Zheng for generating the cDNA construct, Xioaping Li for assistance in protein purification, Dr. Yonis Ahmed for his advice on Hammett plot analysis, David Hoetker for ESI-MS experiments, and Dan Riggs for assistance with HPLC assays.

SUPPORTING INFORMATION AVAILABLE

Parameters obtained from the multivariate regression analysis of Hammett plots as described in the text (Table 1). This material is available free of charge via the Internet at http://pubs.acs.org.

REFERENCES

1. Gutman, G. A., Chandy, K. G., Grissmer, S., Lazdunski, M., McKinnon, D., Pardo, L. A., Robertson, G. A., Rudy, B., Sanguinetti, M. C., Stuhmer, W., and Wang, X. (2005) International Union of Pharmacology. LIII. Nomenclature and molecular relationships of voltage-gated potassium channels. *Pharmacol. Rev. 57* (4), 473–508.
2. Dodson, P. D., and Forsythe, I. D. (2004) Presynaptic K^+ channels: Electrifying regulators of synaptic terminal excitability. *Trends Neurosci. 27* (4), 210–217.
3. Hille, B. (1992) *Ionic Channels of Excitable Membranes*, Sinauer, Sutherland, MA.
4. Jentsch, T. J. (2000) Neuronal KCNQ potassium channels: Physiology and role in disease. *Nat. Rev. Neurosci. 1* (1), 21–30.
5. Krick, S., Platoshyn, O., Sweeney, M., Kim, H., and Yuan, J. X. (2001) Activation of K^+ channels induces apoptosis in vascular smooth muscle cells. *Am. J. Physiol. 280* (4), C970–C979.
6. Ekhterae, D., Platoshyn, O., Krick, S., Yu, Y., McDaniel, S. S., and Yuan, J. X. (2001) Bcl-2 decreases voltage-gated K^+ channel activity and enhances survival in vascular smooth muscle cells. *Am. J. Physiol. 281* (1), C157–C165.
7. Ekhterae, D., Platoshyn, O., Zhang, S., Remillard, C. V., and Yuan, J. X. (2003) Apoptosis repressor with caspase domain inhibits cardiomyocyte apoptosis by reducing K^+ currents. *Am. J. Physiol. 284* (6), C1405–C1410.
8. George, C. K., Wulff, H., Beeton, C., Pennington, M., Gutman, G. A., and Cahalan, M. D. (2004) K^+ channels as targets for specific immunomodulation. *Trends Pharmacol. Sci. 25* (5), 280–289.
9. Farber, G. K., and Petsko, G. A. (1990) The evolution of α/β barrel enzymes. *Trends Biochem. Sci. 15* (6), 228–234.
10. Bachur, N. R. (1976) Cytoplasmic aldo-keto reductases: A class of drug metabolizing enzymes. *Science 193* (4253), 595–597.
11. Jez, J. M., Bennett, M. J., Schlegel, B. P., Lewis, M., and Penning, T. M. (1997) Comparative anatomy of the aldo-keto reductase superfamily. *Biochem. J. 326* (Part 3), 625–636.
12. Gulbis, J. M., Mann, S., and MacKinnon, R. (1999) Structure of a voltage-dependent K^+ channel β subunit. *Cell 97* (7), 943–952.
13. McCormack, T., and McCormack, K. (1994) Shaker K^+ channel β subunits belong to an NAD(P)H-dependent oxidoreductase superfamily. *Cell 79* (7), 1133–1135.
14. Liu, S. Q., Jin, H., Zacarias, A., Srivastava, S., and Bhatnagar, A. (2001) Binding of pyridine nucleotide coenzymes to the β-subunit of the voltage-sensitive K^+ channel. *J. Biol. Chem. 276* (15), 11812–11820.
15. Tipparaju, S. M., Liu, S. Q., Barski, O. A., and Bhatnagar, A. (2007) NADPH binding to β-subunit regulates inactivation of voltage-gated K^+ channels. *Biochem. Biophys. Res. Commun. 359* (2), 269–276.
16. Tipparaju, S. M., Saxena, N., Liu, S. Q., Kumar, R., and Bhatnagar, A. (2005) Differential regulation of voltage-gated K^+ channels by oxidized and reduced pyridine nucleotide coenzymes. *Am. J. Physiol. 288* (2), C366–C376.
17. Weir, E. K., Lopez-Barneo, J., Buckler, K. J., and Archer, S. L. (2005) Acute oxygen-sensing mechanisms. *N. Engl. J. Med. 353* (19), 2042–2055.
18. Weng, J., Cao, Y., Moss, N., and Zhou, M. (2006) Modulation of voltage-dependent Shaker family potassium channels by an aldo-keto reductase. *J. Biol. Chem. 281* (22), 15194–15200.
19. Bahring, R., Milligan, C. J., Vardanyan, V., Engeland, B., Young, B. A., Dannenberg, J., Waldschutz, R., Edwards, J. P., Wray, D., and Pongs, O. (2001) Coupling of voltage-dependent potassium channel inactivation and oxidoreductase active site of Kvβ subunits. *J. Biol. Chem. 276* (25), 22923–22929.
20. Bradford, M. M. (1976) A rapid and sensitive method for the quantitation of microgram quantities of protein utilizing the principle of protein-dye binding. *Anal. Biochem. 72*, 248–254.
21. Barski, O. A., Gabbay, K. H., Grimshaw, C. E., and Bohren, K. M. (1995) Mechanism of human aldehyde reductase: Characterization of the active site pocket. *Biochemistry 34* (35), 11264–11275.
22. Bhatnagar, A., Liu, S. Q., and Srivastava, S. K. (1991) Structure-activity correlations in human kidney aldehyde reductase-catalyzed reduction of para-substituted benzaldehyde by 3-acetyl pyridine adenine dinucleotide phosphate. *Biochim. Biophys. Acta 1077* (2), 180–186.
23. Srivastava, S., Spite, M., Trent, J. O., West, M. B., Ahmed, Y., and Bhatnagar, A. (2004) Aldose reductase-catalyzed reduction of aldehyde phospholipids. *J. Biol. Chem. 279* (51), 53395–53406.
24. Bligh, E. G., and Dyer, W. J. (1959) A Rapid method of total lipid extraction and purification. *Can. J. Biochem. Physiol. 37*, 911–917.
25. Srivastava, S., Chandra, A., Wang, L. F., Seifert, W. E., Jr., DaGue, B. B., Ansari, N. H., Srivastava, S. K., and Bhatnagar, A. (1998) Metabolism of the lipid peroxidation product, 4-hydroxy-trans-2-nonenal, in isolated perfused rat heart. *J. Biol. Chem. 273* (18), 10893–10900.
26. Charton, M. (1977) Steric Effects. 8. Racemization of Chiral Biphenyls. *J. Org. Chem. 42* (14), 2528–2529.
27. Hansch, C., Leo, A., and Hoekman, D. H. (1995) *Exploring QSAR: Fundamentals and Application in Chemistry and Biology*, American Chemical Society, Washington, DC.
28. Page, M. I. (1984) *The Chemistry of Enzyme Action*, Elsevier Science, New York.
29. Mayr, P., and Nidetzky, B. (2002) Catalytic reaction profile for NADH-dependent reduction of aromatic aldehydes by xylose reductase from *Candida tenuis*. *Biochem. J. 366* (Part 3), 889–899.
30. Bohren, K. M., Grimshaw, C. E., Lai, C. J., Harrison, D. H., Ringe, D., Petsko, G. A., and Gabbay, K. H. (1994) Tyrosine-48 is the proton donor and histidine-110 directs substrate stereochemical selectivity in the reduction reaction of human aldose reductase: Enzyme kinetics and crystal structure of the Y48H mutant enzyme. *Biochemistry 33* (8), 2021–2032.
31. Pawlowski, J. E., and Penning, T. M. (1994) Overexpression and mutagenesis of the cDNA for rat liver 3 α-hydroxysteroid/dihydrodiol dehydrogenase. Role of cysteines and tyrosines in catalysis. *J. Biol. Chem. 269* (18), 13502–13510.
32. Spite, M., Baba, S. P., Ahmed, Y., Barski, O. A., Nijhawan, K., Petrash, J. M., Bhatnagar, A., and Srivastava, S. (2007) Substrate specificity and catalytic efficiency of aldo-keto reductases with phospholipid aldehydes. *Biochem. J. 405* (1), 95–105.
33. Bohren, K. M., Page, J. L., Shankar, R., Henry, S. P., and Gabbay, K. H. (1991) Expression of human aldose and aldehyde reductases. Site-directed mutagenesis of a critical lysine 262. *J. Biol. Chem. 266* (35), 24031–24037.
34. O'Connor, T., Ireland, L. S., Harrison, D. J., and Hayes, J. D. (1999) Major differences exist in the function and tissue-specific expression of human aflatoxin B1 aldehyde reductase and the principal human aldo-keto reductase AKR1 family members. *Biochem. J. 343*, t-504.
35. Vander, J. D., Robinson, B., Taylor, K. K., and Hunsaker, L. A. (1992) Reduction of trioses by NADPH-dependent aldo-keto reductases. Aldose reductase, methylglyoxal, and diabetic complications. *J. Biol. Chem. 267* (7), 4364–4369.
36. Barski, O. A., Papusha, V. Z., Kunkel, G. R., and Gabbay, K. H. (2004) Regulation of aldehyde reductase expression by STAF and CHOP. *Genomics 83* (1), 119–129.
37. Srivastava, S., Chandra, A., Bhatnagar, A., Srivastava, S. K., and Ansari, N. H. (1995) Lipid peroxidation product, 4-hydroxynonenal and its conjugate with GSH are excellent substrates of bovine lens aldose reductase. *Biochem. Biophys. Res. Commun. 217* (3), 741–746.
38. Wang, S., Gustafson, E., Pang, L., Qiao, X., Behan, J., Maguire, M., Bayne, M., and Laz, T. (2000) A novel hepatointestinal leukotriene B4 receptor. Cloning and functional characterization. *J. Biol. Chem. 275* (52), 40686–40694.
39. Yoshimoto, T., and Takahashi, Y. (2002) Arachidonate 12-lipoxygenases. *Prostaglandins Other Lipid Mediators 68−69*, 245–262.
40. Kliewer, S. A., Lenhard, J. M., Willson, T. M., Patel, I., Morris, D. C., and Lehmann, J. M. (1995) A prostaglandin J_2 metabolite

binds peroxisome proliferator-activated receptor γ and promotes adipocyte differentiation. *Cell 83* (5), 813–819.

41. Tsakadze, N. L., Srivastava, S., Awe, S. O., Adeagbo, A. S., Bhatnagar, A., and D'Souza, S. E. (2003) Acrolein-induced vasomotor responses of rat aorta. *Am. J. Physiol. 285* (2), H727–H734.
42. Bhatnagar, A. (1995) Electrophysiological effects of 4-hydroxynonenal, an aldehydic product of lipid peroxidation, on isolated rat ventricular myocytes. *Circ. Res. 76* (2), 293–304.
43. Leitinger, N., Watson, A. D., Faull, K. F., Fogelman, A. M., and Berliner, J. A. (1997) Monocyte binding to endothelial cells induced by oxidized phospholipids present in minimally oxidized low density lipoprotein is inhibited by a platelet activating factor receptor antagonist. *Adv. Exp. Med. Biol. 433*, 379–382.
44. Grimshaw, C. E., Bohren, K. M., Lai, C. J., and Gabbay, K. H. (1995) Human aldose reductase: Rate constants for a mechanism including interconversion of ternary complexes by recombinant wild-type enzyme. *Biochemistry 34* (44), 14356–14365.
45. Jin, Y., and Penning, T. M. (2006) Multiple steps determine the overall rate of the reduction of 5α-dihydrotestosterone catalyzed by human type 3 3α-hydroxysteroid dehydrogenase: Implications for the elimination of androgens. *Biochemistry 45* (43), 13054–13063.
46. Kubiseski, T. J., Hyndman, D. J., Morjana, N. A., and Flynn, T. G. (1992) Studies on pig muscle aldose reductase. Kinetic mechanism and evidence for a slow conformational change upon coenzyme binding. *J. Biol. Chem. 267* (10), 6510–6517.
47. Gulbis, J. M., Zhou, M., Mann, S., and MacKinnon, R. (2000) Structure of the cytoplasmic β subunit-T1 assembly of voltage-dependent K^+ channels. *Science 289* (5476), 123–127.
48. Schlegel, B. P., Jez, J. M., and Penning, T. M. (1998) Mutagenesis of 3α-hydroxysteroid dehydrogenase reveals a "push-pull" mechanism for proton transfer in aldo-keto reductases. *Biochemistry 37* (10), 3538–3548.
49. Tarle, I., Borhani, D. W., Wilson, D. K., Quiocho, F. A., and Petrash, J. M. (1993) Probing the active site of human aldose reductase. Site-directed mutagenesis of Asp-43, Tyr-48, Lys-77, and His-110. *J. Biol. Chem. 268* (34), 25687–25693.
50. Kratzer, R., Kavanagh, K. L., Wilson, D. K., and Nidetzky, B. (2004) Studies of the enzymic mechanism of *Candida tenuis* xylose reductase (AKR 2B5): X-ray structure and catalytic reaction profile for the H113A mutant. *Biochemistry 43* (17), 4944–4954.
51. Long, S. B., Campbell, E. B., and MacKinnon, R. (2005) Crystal structure of a mammalian voltage-dependent Shaker family K^+ channel. *Science 309* (5736), 897–903.
52. Perez-Garcia, M. T., Lopez-Lopez, J. R., and Gonzalez, C. (1999) Kvβ1.2 subunit coexpression in HEK293 cells confers O_2 sensitivity to Kv4.2 but not to Shaker channels. *J. Gen. Physiol. 113* (6), 897–907.

BI800301B